Journal of Colloid and Interface Science 531 (2018) 74–82

Contents lists available at ScienceDirect

Journal of Colloid and Interface Science

journal homepage: www.elsevier.com/locate/jcis

Regular Article

Gas sensor based on samarium oxide loaded mulberry-shaped tin oxide for highly selective and sub ppm-level acetone detection

Yiqun Zhang, Linsheng Zhou, Yueying Liu, Deye Liu, Fengmin Liu *, Fangmeng Liu, Xu Yan, Xishuang Liang, Yuan Gao, Geyu Lu *

State Key Laboratory of Integrated Optoelectronics, Key Laboratory of Gas Sensors, Jilin Province and College of Electronic Science and Engineering, Jilin University, 2699 Qianjin Street, Changchun 130012, People's Republic of China

GRAPHICAL ABSTRACT

The dynamical response-recovery curves of the sensors based on the pure SnO_2 and 2.5 mol% Sm_2O_3/SnO_2 to different concentrations of acetone.

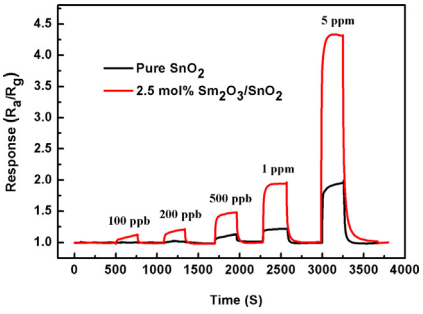

ARTICLE INFO

Article history:
Received 15 May 2018
Revised 12 July 2018
Accepted 12 July 2018
Available online 17 July 2018

Keywords:
Sm_2O_3
SnO_2
Mulberry-shaped
Gas sensor
Acetone

ABSTRACT

Mulberry-shaped tin oxide (SnO_2) hierarchical architectures and samarium oxide (Sm_2O_3) loaded tin oxide with different amounts (0.5, 1, 2.5, and 4 mol% Sm_2O_3) were successfully synthesized by facile hydrothermal synthesis method and simple isometric impregnation method. The gas sensing performance of the sensors based on pure SnO_2 and Sm_2O_3 loaded SnO_2 materials were systematically investigated. The results indicated that Sm_2O_3 loading considerably affected the improvement of the sensing performance of the SnO_2 sensor. The 2.5 mol% Sm_2O_3/SnO_2 exhibited the highest response (41.14) to 100 ppm acetone, the response was 2.29 times higher than that of pure SnO_2 (18). In addition, with 2.5 mol% Sm_2O_3 loading, the low detection threshold of the sensor dropped from 500 ppb to 100 ppb. The enhanced gas sensing performance was mainly bacause of the increased oxygen vacancies created by the substitution of samarium in the SnO_2 lattice, which enhanced the adsorption of oxygen and the exceptional catalytic effect of Sm_2O_3.

1. Introduction

In recent years, the monitoring demand of toxic pollutant gases has been growing bacause of their wide-ranging applications in air quality control, environmental protection, healthcare, and security [1–5]. As a common type of volatile organic chemical (VOC),

* Corresponding authors.
E-mail addresses: liufm@jlu.edu.cn (F. Liu), lugy@jlu.edu.cn (G. Lu).

https://doi.org/10.1016/j.jcis.2018.07.052
0021-9797/

acetone is widely used in laboratories and industries [6,7]. However, long-term exposure to acetone can harm the nervous system and organs [8,9]. Furthermore, the concentration of acetone in respiration can be used as a key biomarker for diabetes diagnosis. As reported by clinical data, a considerable difference occurs in the exhaled acetone concentration between a healthy person and a diabetic patient, the concentration of exhaled acetone is 0.3–0.9 ppm for a healthy individual, and more than 1.8 ppm for a diabetic patient [10,11]. Therefore, it is of significance to develop a acetone sensor with high sensitivity and low detection limit for environmental protection and biomedical applications.

In the past few decades, gas sensors based on semiconductor oxide have attracted researchers worldwide because of their simple device structure, miniaturization, good reproducibility, fast response, real-time detection and low cost [12–14]. Semiconductor oxides, such as ZnO, SnO_2 WO_3 and In_2O_3, are important materials widely applied as gas sensing materials and exhibited excellent sensing properties [15–18]. Among these materials, SnO_2, as a wide band gap (3.6 eV) *n*-type semiconductor, is a proper candidate for potential applications in the gas sensing field because of its high sensitivity, low operating temperatures (200–400 °C), and good long term stability [19,20]. To date, various synthesized methods have been successfully exploited for the preparation of SnO_2, such as hydrothermal/solvothermal synthesis method [21,22], high current heating [23], sol-gel [24,25], template-assisted method [26], electrospinning [27,28], and chemical precipitation [29].

However, the gas sensing properties of single SnO_2 hardly meet all the requirements of gas sensors, and therefore restrict their practical application and development. Thus, scientific and technological efforts have been exerted to improve the gas sensing performance of SnO_2, doping/loading with suitable noble metals or metal oxides have been proved to be a simple and efficient route to enhance the sensing properties of semiconductor gas sensors [30–33]. Samarium, as a rare earth element, has special optical, electronic and magnetic properties [34]. Samarium ion with 4f electronic configuration usually exists in the form of Sm^{3+} [35,36], which has been proven to have fast oxygen ion mobility and predominant catalytic properties in previous studies [37,38].

In this work, we prepared mulberry-shaped SnO_2 hierarchical architectures and Sm_2O_3 loaded SnO_2 via facile hydrothermal synthesis method and simple isometric impregnation route. The gas sensing properties of the above materials were systematically investigated to examine the best Sm_2O_3 loading amount and the enhanced effect of Sm_2O_3 on the gas sensing properties of SnO_2 based acetone sensor.

2. Experimental

2.1. Synthesis of mulberry-shaped SnO_2 and loading with Sm_2O_3

All the reagents (analytical-grade purity) were purchased and used without any further purification. The initial precursors were tin (II) chloride dihydrate ($SnCl_2{\cdot}2H_2O$, ≥98.0%, Sinopharm Chemical Reagent Co., Ltd, China), samarium nitrate hexahydrate ($Sm(NO_3)_3{\cdot}6H_2O$, 99.99%, Sahn Chemical Technology (Shanghai) Co., Ltd, China) and ammonium sulfate ($(NH_4)_2SO_4$, ≥99.0%, Sinopharm Chemical Reagent Co., Ltd, China). For the synthesis of SnO_2 materials, the hydrothermal synthesis method [6,32] was introduced. The detailed process was as follows: A total of 0.15 g $(NH_4)_2SO_4$ was dissolved into a mixture of ethanol and water (1:1, v/v) with vigorous stirring to form a homogeneous solution. Then, 0.677 g $SnCl_2{\cdot}2H_2O$ was added into the above solution. The resulting mixture was subsequently transferred into a Teflon-lined stainless steel autoclave and reacted at 120 °C for 8 h. Finally, the precipitate was centrifuged, washed, dried at 80 °C and calcined at 500 °C for 2 h.

After SnO_2 materials were obtained, Sm_2O_3 was loaded on SnO_2 by isometric impregnation [39]. The preparation details were shown as follows: the maximum volume of samarium nitrate solution absorbed by SnO_2 powder was dropped into 0.05 g SnO_2 at room temperature and steeped for 4 h. The concentrations of samarium nitrate solution were adjusted on the basis of the loading amount of Sm_2O_3. Finally, the products were dried and calcined at 500 °C for 2 h. The samples were named 0.5, 1, 2.5, and 4 mol% Sm_2O_3/SnO_2.

2.2. Characterization of samples

X-ray diffraction (XRD, Rigaku D/max-2550 diffractometer, Cu kα radiation at wavelength λ = 0.1541 nm) was carried out to analyze the crystalline phases of the as-synthesized products, The morphologies and structures of the samples were recorded by field emission scanning electron microscopy (SEM, JEOLJSM-7500F), transmission electron microscopy (TEM, JEOL JEM-2100F), high-resolution transmission electron microscopy (HRTEM) and energy dispersive X-ray spectroscopic (EDS) elemental mapping

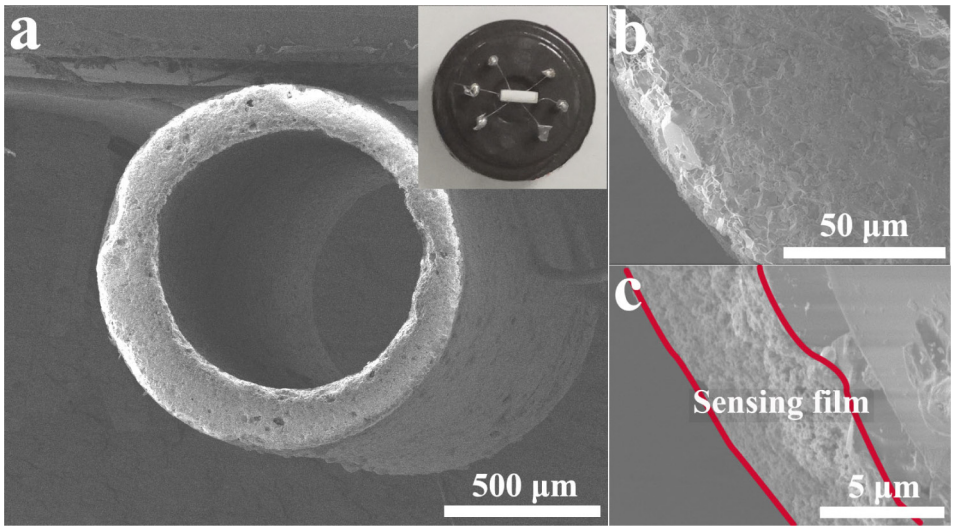

Fig. 1. The cross-section view of SEM images for the sensing film.

measurements. For surface properties study, the Brunauer-Emmett-Teller (BET) specific surface areas of the samples were measured by nitrogen adsorption measurements (Gemini VII 2390), and the X-ray photoelectron spectroscopy (XPS) experiments with monochromatic Al Kα source were performed. All the binding energies were calibrated in reference to the signal adventitious carbon C1s peak (284.8 eV).

2.3. Fabrication and measurement of the sensors

The as-prepared samples (0.05 g) were made into slurry form by mixing with 0.15 ml deionized water, and then the slurry was coated onto the outside surface of an alumina tube with a pair of gold electrodes [22]. The sensing devices were dried for 30 min under IR radiation and sintered at 400 °C for 2 h. The working temperature of the sensor was controlled by modulating the power of the Ni-Cr alloy coil heater which was inserted in the alumina tube. The photograph of the gas sensor and the cross-section view of SEM images for the sensing film were shown in Fig. 1, the thickness of the sensing film was about 3.8–5.2 μm. In order to measure the sensing performance, the sensor was put into a closed chamber, and then a required amount of target gas was injected into the chamber and mixed with air, when the response reached a constant value, the test gas was removed and replaced by air. The gas response was defined as $S = R_a/R_g$ for reducing gas, where R_a and R_g were defined as the resistance in air and the target gas, respectively. The response time and recovery time was defined as the time taken by the sensor to achieve 90% of the total resistance change in the case of adsorption or desorption, respectively.

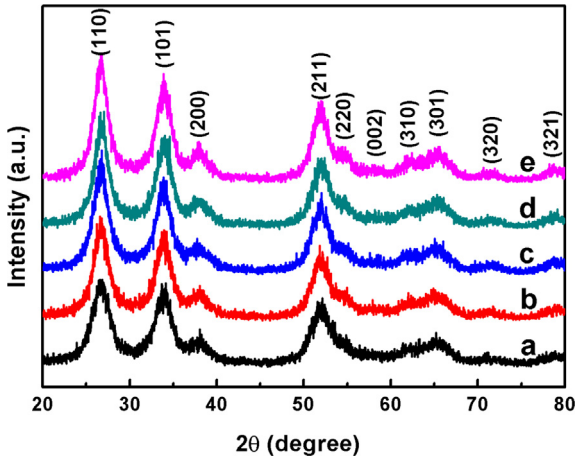

Fig. 2. The XRD patterns of pure SnO_2 (a) and Sm_2O_3 loaded SnO_2 materials with various Sm_2O_3 amounts (b, 0.5 mol%; c, 1 mol%, d, 2.5 mol%; e, 4 mol%).

3. Results and discussion

3.1. Characterizations of obtained materials

The XRD patterns of pure SnO_2 and Sm_2O_3 loaded SnO_2 materials with various Sm_2O_3 amounts are shown in Fig. 2. Evidently, all the diffraction peaks of the as-prepared samples could be well indexed as the tetragonal rutile structure of SnO_2 with lattice parameters of a = 0.4738 nm and c = 0.3187 nm, which was in good accordance with the standard data file (JCPDS File No. 41-1445). No diffraction peaks that correspond to samarium oxide were observed, even when the Sm_2O_3 content was 4 mol%, which reveals that it may be amorphous or its crystallites were too small to be detected by XRD.

SEM and TEM measurements were conducted to further obtain the detailed information of morphologies about pure SnO_2 and Sm_2O_3 loaded SnO_2 materials. SEM image of the as-prepared pure SnO_2 sample is shown in Fig. 3a, in which many mulberry-shaped SnO_2 architectures were observed, as can be seen the mulberry-shaped architectures have a diameter of approximately 50–150 nm, and the entire area was constituted by the stacking of nanoparticles with diameters of approximately 4–10 nm. They were closed to each other, and stacked toghter, thereby forming the mulberry-shaped hierarchical architecture, and endowing the material with a porous structure, which is potentially beneficial for the diffusion and transport of gas molecules. SEM images of the Sm_2O_3 loaded SnO_2 materials are shown in Fig. 3b–e. Sm_2O_3 loading had nearly no influence on the morphology, and the 3D hierarchical nanostructure of pure SnO_2 was maintained after Sm_2O_3 loading. Fig. 4 shows the TEM, HRTEM and EDS information of 2.5 mol% Sm_2O_3/SnO_2 material. The low-magnification TEM image is shown in Fig. 4a and the high-magnification TEM image of an independent mulberry-shaped architecture is shown in

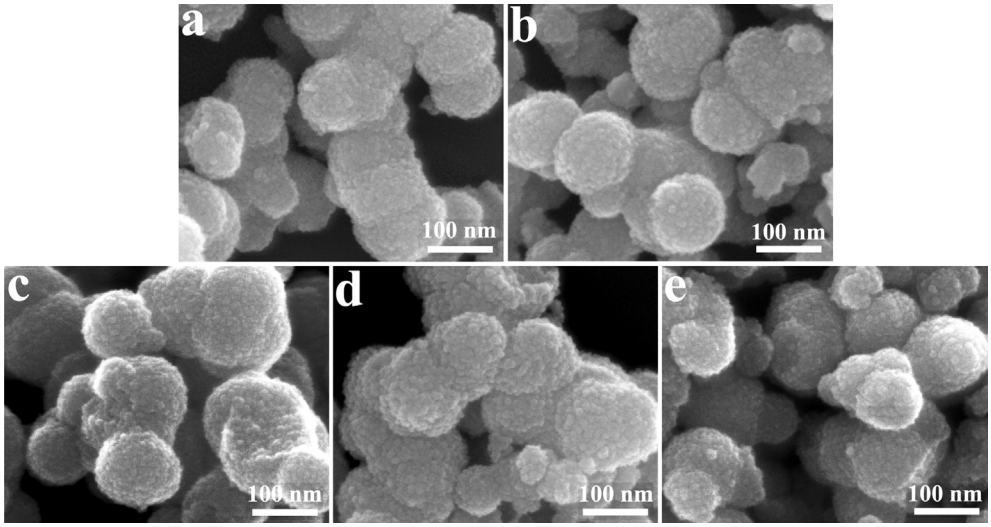

Fig. 3. SEM images of pure SnO_2 (a), 0.5 mol% (b), 1 mol% (c), 2.5 mol% (d) and 4 mol% (e) Sm_2O_3 loaded SnO_2 materials.

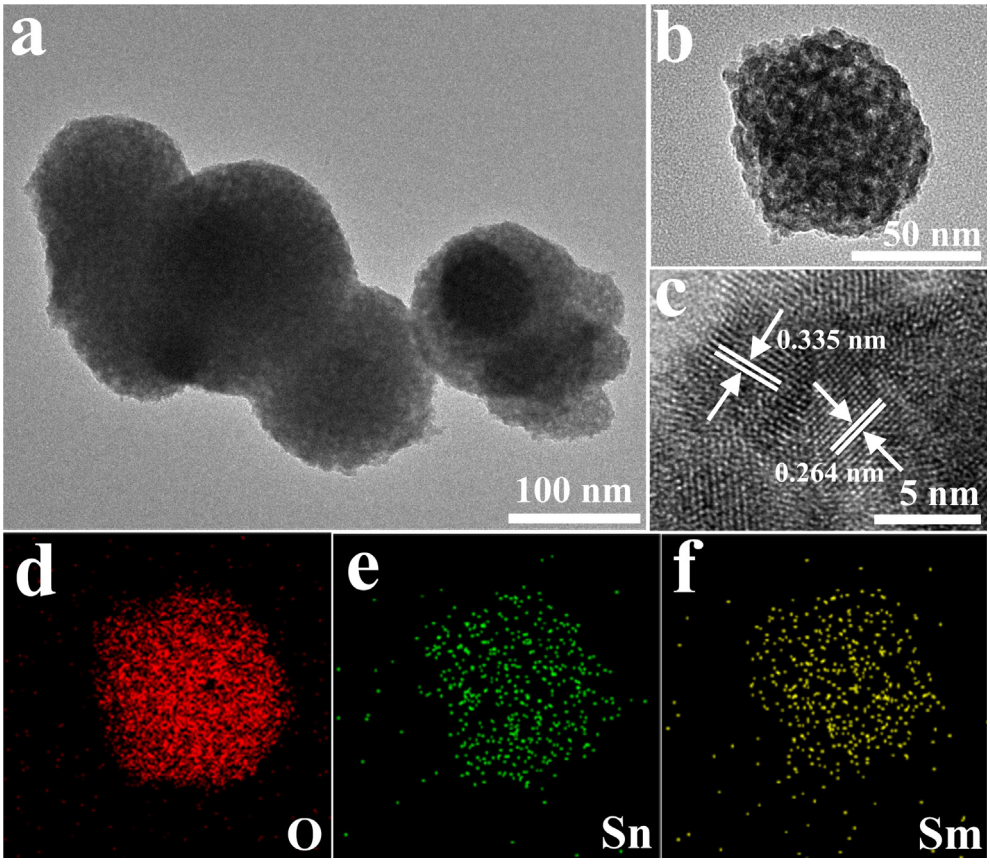

Fig. 4. TEM images (a, b) and HRTEM image (c) of 2.5 mol% Sm_2O_3/SnO_2; (d–f) elemental mapping of individual mulberry-shaped architecture shown in Fig. 3b.

Fig. 4b. From the HRTEM image of 2.5 mol% Sm_2O_3/SnO_2 (Fig. 4c), it could be calculated that the lattice spacings were about 0.335 nm and 0.264 nm, which corresponded to the (1 1 0) and (1 0 1) planes of SnO_2. Besides the morphology of the Sm_2O_3/SnO_2 material, corresponding EDS elemental mappings of the individual 2.5 mol% Sm_2O_3/SnO_2 mulberry-shaped architecture (Fig. 4b) were also characterized, as shown in Fig. 4d–f. It is obvious that the mulberry-shaped nanostructure consisted of O, Sn and Sm elements, and Sm was distributed uniformly on the entire surface of the SnO_2 hierarchical nanostructure.

The BET-specific surface areas, average pore sizes and pore volumes of pure SnO_2 and Sm_2O_3 loaded SnO_2 materials are listed in Table 1. The specific surface areas decreased remarkably with an increase in Sm_2O_3 loading amount because more SnO_2 surfaces were covered. The surface area of pure SnO_2 and 0.5, 1, 2.5, 4 mol% Sm_2O_3/SnO_2 are calculated to be 78.98, 72.19, 62.01, 54.11, 22.55 $m^2\ g^{-1}$, respectively. With the increase in Sm_2O_3 loading amount, the pore volume slightly decreased and the average pore size slightly increased.

To further illuminate the composition and the chemical state of the elements on the surface of the as-prepared samples, XPS analyses were performed. Fig. 5a shows the wide survey spectrum of the 2.5 mol% Sm_2O_3/SnO_2 material. The characteristic peaks of C, Sn, O, and Sm could be clearly observed, and no impurities could be found, which indicated the high purity of the sample. Fig. 5b displays the high-resolution XPS spectra of Sm 3d of 2.5 mol% Sm_2O_3/SnO_2. The binding energy of Sm $3d_{5/2}$ was approximately 1083.9 eV, which confirms that the valence state of Sm was +3. Fig. 5c, d show the XPS survey spectra of Sn 3d and O 1s for the pure SnO_2 and 2.5 mol% Sm_2O_3/SnO_2 samples. There were two strong peaks centered at 487.8 eV and 496.2 eV for pure SnO_2 in Fig. 5c, they could be respectively indexed to the characteristic spin-orbit split states of Sn $3d_{5/2}$ and Sn $3d_{3/2}$, thereby indicating a Sn oxidation state of +4. Furthermore, the binding energy for the 2.5 mol% Sm_2O_3/SnO_2 sample decreased by 0.7 eV compared with that of the pure SnO_2 sample (from 487.8 eV to 487.1 eV for Sn $3d_{5/2}$ and from 496.2 eV to 495.5 eV for Sn $3d_{3/2}$). In addition, as shown in Fig. 5d, a chemical shift of binding energy for O 1s toward the low energy direction also occurred for the 2.5 mol% Sm_2O_3/SnO_2 sample, thereby indicating that some Sm components were incorporated into the SnO_2 lattice.

Table 1
Textural properties of SnO_2 and Sm_2O_3 loaded SnO_2 materials.

Sample	Specific surface area ($m^2\ g^{-1}$)	Average pore size (nm)	Pore volume ($cm^3\ g^{-1}$)
Pure SnO_2	78.98	7.85	0.1511
0.5 mol% Sm_2O_3/SnO_2	72.19	8.32	0.1545
1 mol% Sm_2O_3/SnO_2	62.01	7.96	0.1210
2.5 mol% Sm_2O_3/SnO_2	54.11	11.27	0.0984
4 mol% Sm_2O_3/SnO_2	22.55	20.91	0.1081

3.2. Gas sensing performance

In order to investigate the effect of Sm_2O_3 loading on the acetone sensing performance of the mulberry-shaped SnO_2 materials, the sensing properties of sensors based on pure SnO_2 and Sm_2O_3 loaded SnO_2 materials with different Sm_2O_3 loading amounts to 100 ppm acetone were measured at 250 °C, as shown in Fig. 6a. The result indicated that the Sm_2O_3 loading amount considerably influenced the response property. The response of the sensor was enhanced with the increase of Sm_2O_3 loading amount. The 2.5

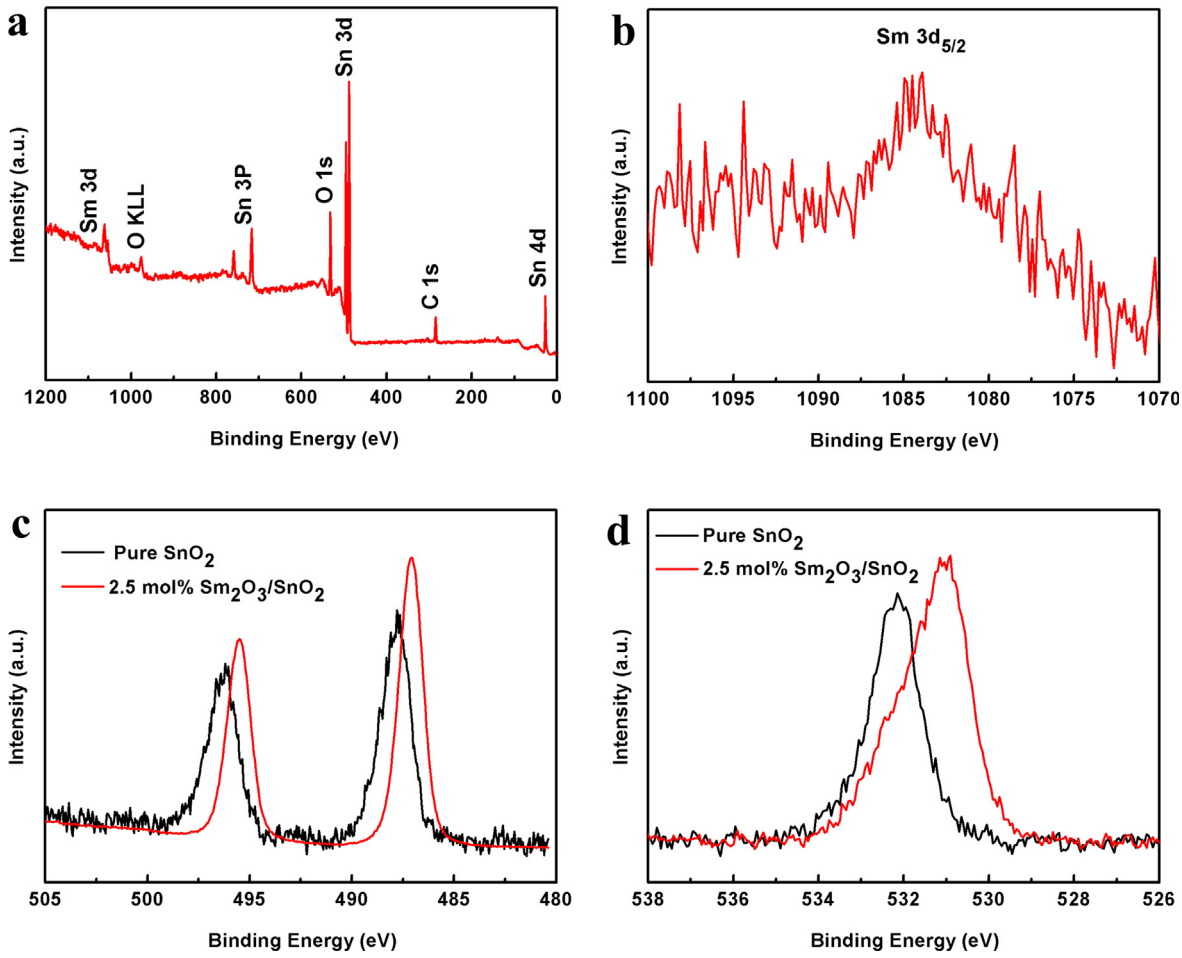

Fig. 5. Wide XPS spectra (a), and Sm 3d (b) of as-prepared 2.5 mol% Sm_2O_3/SnO_2 sample, Sn 3d (c), and O 1s (d) of pure SnO_2 and 2.5 mol% Sm_2O_3/SnO_2 samples.

mol% Sm_2O_3/SnO_2 exhibited the highest response (41.14) to 100 ppm acetone, the response was 2.29 times higher than that of pure SnO_2 (18). However, when Sm_2O_3 loading amount increased continually, the response of the sensor began to decrease. This phenomenon could be explained by the excess amount of Sm_2O_3 occupied the limited active sites of the SnO_2 surface, thereby preventing the acetone molecules from reacting with adsorbed oxygen species. Fig. 6b shows the gas response of the sensors based on pure SnO_2 and 2.5 mol% Sm_2O_3/SnO_2 composites to 100 ppm acetone measured at different temperatures. Evidently, 2.5 mol% Sm_2O_3/SnO_2 exhibited the highest response at 250 °C, which was used as the operating temperature in all the succeeding investigations. Fig. 6c shows the resistance of pure SnO_2 and 2.5 mol% Sm_2O_3/SnO_2 sensors in air at different temperatures. After Sm_2O_3 loading, the resistance of the sensor in air increased tremendously by more than two orders of magnitude. The resistance (R) can be described with the following expression:

$$R = k_1R_V + k_2R_S \quad (1)$$

Here, k_1 and k_2 are constants, R_V represents the body resistance and R_S stands for the surface resistance. Given that R_V is far less than R_S, the expression (1) can be simplified to (2) as follows:

$$R = k_2R_S \quad (2)$$

When Sm_2O_3 load on SnO_2, the number of grain boundaries will be increased, thereby resulting in an increase in the total value of surface resistance. In addition, oxygen vacancies created by the substitution of samarium in the SnO_2 lattice will enhance the adsorption of oxygen and further increase the barrier height in the grain boundaries. These factors lead to an increase in resistance eventually. Notably, after Sm_2O_3 loading, the influence of the temperature on the resistance of the sensor became minimal, which is favorable in practical application. The response and recovery properties are also significant characteristics of gas sensor for real-time monitoring. The transient response and recovery curves of pure SnO_2 and 2.5 mol% Sm_2O_3/SnO_2 based sensors are shown in Fig. 6d. Sm_2O_3 loading has no strong influence on response and recovery properties. Both sensors exhibited fast response and quick recovery toward 100 ppm acetone.

The response of the sensors based on pure SnO_2 and 2.5 mol% Sm_2O_3/SnO_2 composites to 0.1–200 ppm acetone was also measured, as shown in Fig. 7a. Obviously, the gas response of the sensor increased with the increasing of the acetone concentration, and maintained a nearly linearly increasing trend in the range of 0.1–200 ppm. Fig. 7b shows the dynamical response-recovery curves of the sensors based on pure SnO_2 and 2.5 mol% Sm_2O_3/SnO_2 toward low acetone concentration (100 ppb–5 ppm). For the pure SnO_2, the low detection limit was 500 ppb. With 2.5 mol% Sm_2O_3 loading, the low detection threshold of the sensor dropped. The sensor continued to have a noticeable response even when the concentration of acetone decreased to 100 ppb. Fig. 7c depicts the continuous response of the MOS sensors that were based on 2.5 mol% Sm_2O_3/SnO_2 to 100 ppm acetone at the operating temperature of 250 °C. Thirty reversible cycles of the response curves suggested that the sensor had excellent repeatable and reversible characteristics to a certain extent. Fig. 7d shows the

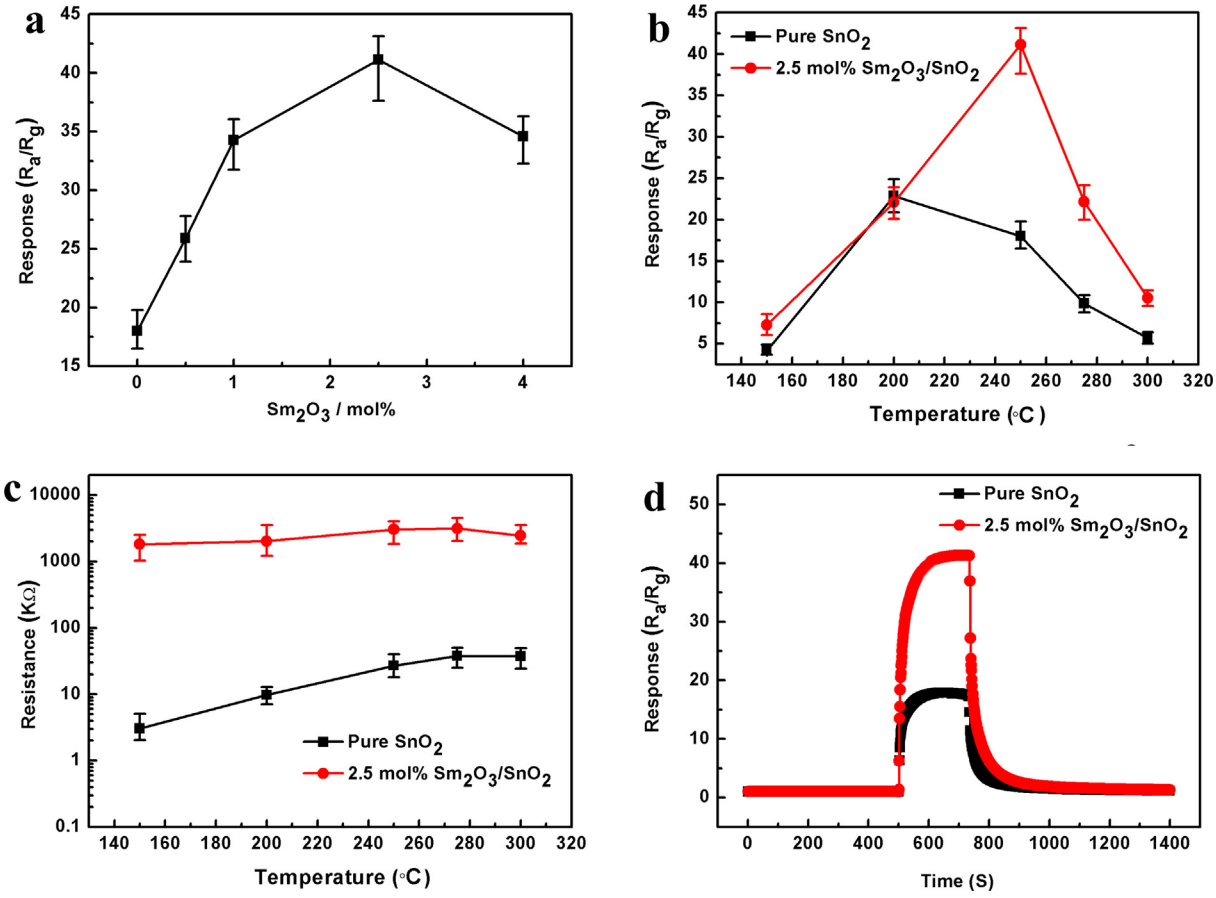

Fig. 6. Response of the sensors based on of pure SnO_2 and Sm_2O_3 loaded SnO_2 materials with different Sm_2O_3 loading amounts (a), responses at different operating temperatures (b) and resistances in air at different temperatures (c) as well as dynamic response curves to 100 ppm acetone of the sensors based on pure SnO_2 and 2.5 mol% Sm_2O_3/SnO_2.

response of the sensors at the operating temperature of 250 °C to various gases, including 100 ppm toluene, methanol, ethanol, acetone and formaldehyde. The 2.5 mol% Sm_2O_3/SnO_2 samples showed enhanced responses for most target gases compared with the pure SnO_2. The response of 2.5 mol% Sm_2O_3/SnO_2 based sensor to acetone was the highest among those of all the tested VOC gases. Table 2 listes the comparison of acetone sensing performance between this work and previously reported results [40–45]. Evidently, the sensor based on 2.5 mol% Sm_2O_3/SnO_2 exhibited good performance, especially the detection limit at low working temperature. The low detection limit is 100 ppb, which is lower than the limit of detecting diabetes, thereby indicating that the sensor based on 2.5 mol% Sm_2O_3/SnO_2 may be a promising candidate for diabetes diagnosis through exhaled breath.

3.3. Gas sensing mechanism

It is well known that the sensing mechanism of metal oxide semiconductor (MOS) gas sensor primarily depends on the resistance change of the sensing material. When SnO_2 based sensor is exposed to air, electrons will transfer from the surface of SnO_2 to adsorbed oxygen, thereby resulting in the formation of an electron depletion layer and a decrease in resistance. Once the sensor is exposed to acetone, acetone will react with the surface oxygen ions and release captured electrons to SnO_2, thereby leading to a thin electron depletion layer and decreased resistance.

Compared with pure SnO_2, the Sm_2O_3/SnO_2 materials demonstrated remarkably enhanced gas sensing performance. A schematic of the gas sensing mechanism is shown in Fig. 8. One key factor for the improved sensitivity was the increased oxygen vacancies created by the substitution of samarium in the SnO_2 lattice, which enhanced the adsorption of oxygen. It is well known that oxygen vacancy considerably influences the gas sensing properties of surface resistance-type metal oxide semiconductors [46,47]. When Sm was introduced into the SnO_2 lattice, Sm^{3+} substituted Sn^{4+}, thereby leading to the formation of oxygen vacancy to maintain electrical neutrality of the structure on the basis of the electronic compensation mechanism, which can be described in the form of the following equation:

$$Sm_2O_3 \xrightarrow{SnO_2} 2Sm'_{Sn} + 3O_O^{\times} + V_O^{\cdot\cdot} \quad (3)$$

Here, Sm'_{Sn} represents the substitution of the site of Sn^{4+} by Sm^{3+} with one negative charge, $O_O^{\times}$ represents a neutral oxygen atom on the oxygen site, and $V_O^{\cdot\cdot}$ denotes oxygen vacancy with two positive charges.

The gas response of the MOS sensor can be written as follows:

$$S = \frac{Ra}{Rg} = \frac{\sigma g}{\sigma a} = \frac{ngq\mu}{naq\mu} = \frac{ng}{na} \quad (4)$$

where σ_a/n_a and σ_g/n_g are the conductance/electron concentrations of the sensing material in air and target gas, q is the charge, and μ represents the electron mobility. When △n is defined as the difference of electron concentration in target and air gas, expression (4) can be changed into (5) as follows:

$$S = \frac{na + \triangle n}{na} = 1 + \frac{\triangle n}{na} \quad (5)$$

When oxygen vacancy is increased, more oxygen will absorb on the surface of the sensing material and capture electrons from

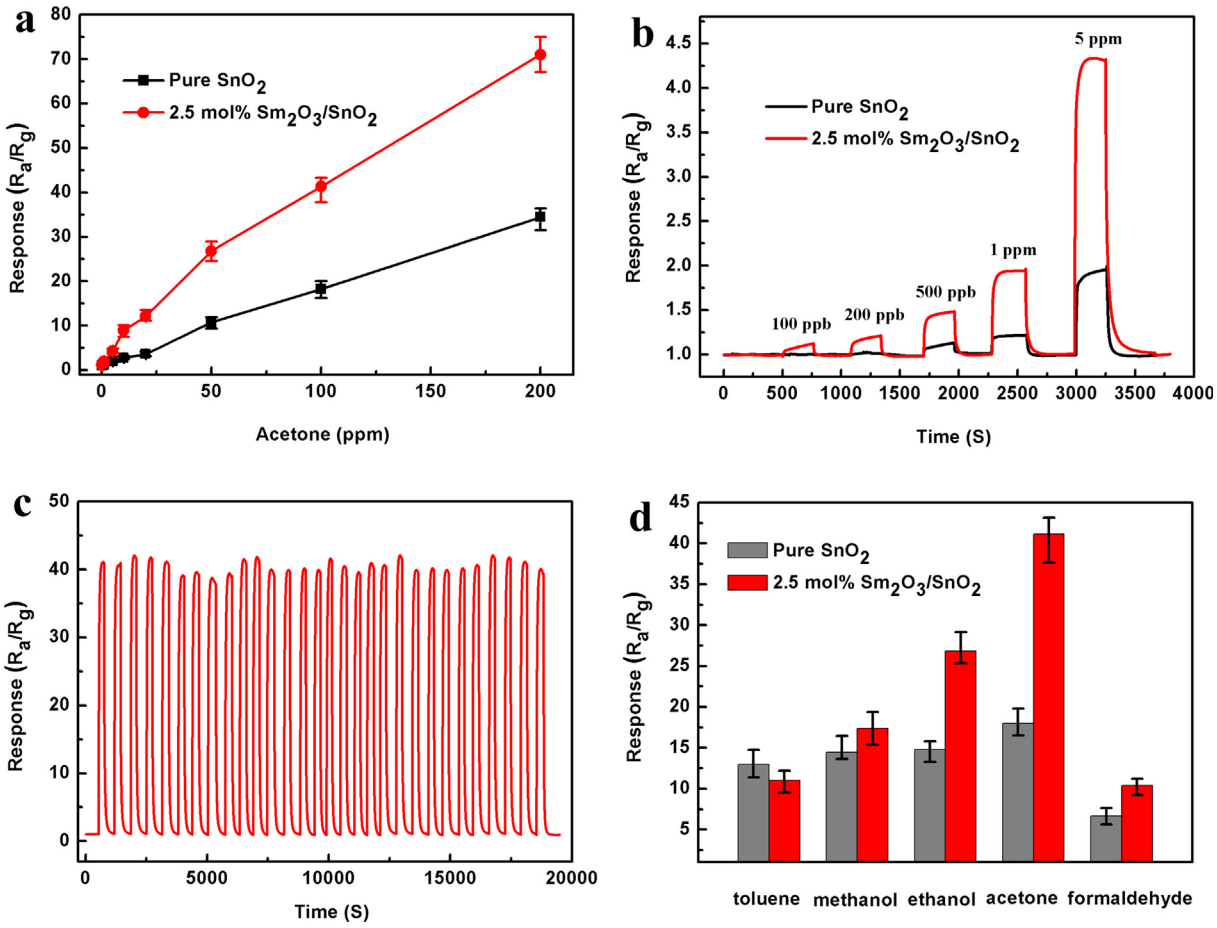

Fig. 7. The responses (a) and dynamical response-recovery curves (b) of the sensors based on pure SnO_2 and 2.5 mol% Sm_2O_3/SnO_2 to different concentrations of acetone, (c) the continuous response of the sensor based on 2.5 mol% Sm_2O_3 to 100 ppm acetone, (d) the response to 100 ppm various gases of the sensors based on the pure SnO_2 and 2.5 mol% Sm_2O_3/SnO_2.

Table 2
The comparison of acetone sensing performances between the this work and previously reported results [40–45].

Sensing materials	Concentration (ppm)	T (°C)	Response	Low detection limit	Reference
$ZnSnO_3/SnO_2$ hollow urchin	50	280	17.03	1 ppm	[40]
WO_3 nanoplates microcubes	1000	300	42	2 ppm	[41]
5 mol% Cr_2O_3-doped WO_3 films	20	320	9	500 ppb	[42]
ZnO nanorods	100	300	30.4	1 ppm	[43]
Pt-WO_3 nanofiber	5	350	8.2	300 ppb	[44]
2 mol% Eu-doped SnO_2 nanofibers	100	280	32.2	300 ppb	[45]
2.5 mol% Sm_2O_3/SnO_2	**100**	**250**	**41.14**	**100 ppb**	**Present work**

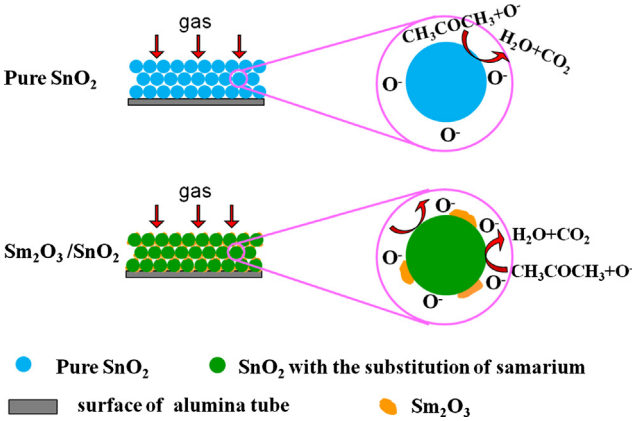

Fig. 8. Schematic of the gas sensing mechanism.

SnO_2, thereby leading to a decrease in electron concentration. In other words, n_a of Sm_2O_3/SnO_2 is lower than that of SnO_2. When the sensor is exposed to acetone, more acetone will react with the surface oxygen ions and release more captured electrons to SnO_2. Thus, $\triangle n$ of Sm_2O_3/SnO_2 is larger than that of SnO_2. The decrease of n_a and the increase of $\triangle n$ help improve the response to acetone. Another important factor is the exceptional catalytic effect of Sm_2O_3, which promotes the reaction between acetone and surface oxygen ion absorbed on SnO_2, and further decreases n_a and increases $\triangle n$. Thus, the response of the sensor is substantially improved.

4. Conclusion

In summary, mulberry-shaped SnO_2 hierarchical architectures and Sm_2O_3 loaded SnO_2 were successfully synthesized by facile

hydrothermal synthesis method and simple isometric impregnation route. The Sm_2O_3 loading materials are crucial in improving the acetone sensing properties of SnO_2 sensor. With 2.5 mol% Sm_2O_3 loading, the response to acetone was increased greatly and the low detection threshold of the sensor dropped from 500 ppb to 100 ppb, which was lower than that in the literature. The low detection threshold meets the need for the limit of detecting diabetes, thereby indicating that the sensor based on 2.5 mol% Sm_2O_3/SnO_2 may be a promising candidate for diabetes diagnosis through exhaled breath. The enhanced gas sensing performance was mainly due to the increased oxygen vacancies created by the substitution of samarium in the SnO_2 lattice, which enhanced the adsorption of oxygen and the exceptional catalytic effect of Sm_2O_3. Thus, the loading of Sm_2O_3 onto mulberry-shaped SnO_2 should be a promising approach for enhancing the performance of SnO_2-based acetone sensor and a effective approach for the early detection of diabetes through exhaled breath.

Acknowledgements

This work was supported by National key Research and Development Program of China (No. 2016YFC0201002), National Nature Science Foundation of China (Nos. 61474057, 61573164, 61520106003), National High-Tech Research and Development Program of China (863 Program, No. 2014AA06A505).

References

[1] M. Lucci, A. Reale, A. Di Carlo, S. Orlanducci, E. Tamburri, M.L. Terranova, I. Davoli, C. Di Natale, A. D' Amico, R. Paolesse, Optimization of a NOx gas sensor based on single Walled carbon nanotubes, Sens. Actuators B 118 (2006) 226–231.
[2] T. Kawano, H.C. Chiamori, M. Suter, Q. Zhou, B.D. Sosnowchik, L.W. Lin, An electrothermal carbon nanotube gas sensor, Nano Lett. 7 (2007) 3686–3690.
[3] R. Barro, J. Regueiro, M. Llompart, C. Garcia-Jares, Analysis of industrial contaminants in indoor air: Part 1. Volatile organic compounds, carbonyl compounds, polycyclic aromatic hydrocarbons and polychlorinated biphenyls, J. Chromatogr. A 1216 (2009) 540–566.
[4] S. Wang, H.M. Ang, M.O. Tade, Volatile organic compounds in indoor environment and photocatalytic oxidation: state of the art, Environ. Int. 33 (2007) 694–705.
[5] S. Salehi, E. Nikana, A.A. Khodadadi, Y. Mortazavi, Highly sensitive carbon nanotubes-SnO_2 nanocomposite sensor for acetone detection in diabetes mellitus breath, Sens. Actuators B: Chem. 205 (2014) 261–267.
[6] J. Hu, J. Yang, W.D. Wang, Y. Xue, Y.J. Sun, P.W. Li, K. Lian, W.D. Zhang, L. Chen, J. Shi, Y. Chen, Synthesis and gas sensing properties of NiO/SnO_2 hierarchical structures toward ppb-level acetone detection, Mater. Res. Bull. 102 (2018) 294–303.
[7] L.K. Bagal, J.Y. Patil, I.S. Mulla, S.S. Suryavanshi, Studies on the resistive response of nickel and cerium doped SnO_2 thick films to acetone vapor, Ceram. Int. 38 (2012) 6171–6179.
[8] K.T. Alali, J.Y. Liu, Qi Liu, R.M. Li, H.Q. Zhang, K. Aljebawi, P.L. Liu, J. Wang, Enhanced acetone gas sensing response of ZnO/$ZnCo_2O_4$ nanotubes synthesized by single capillary electrospinning technology, Sens. Actuators B: Chem 252 (2017) 511–522.
[9] S.B. Upadhyay, R.K. Mishra, P.P. Sahay, Enhanced acetone response in co-precipitated WO_3 nanostructures upon indium doping, Sens. Actuators B: Chem. 209 (2015) 368–376.
[10] R.Q. Xing, Q.L. Li, L. Xia, J. Song, L. Xu, J.H. Zhang, Y. Xie, H.W. Song, Au-modified three-dimensional In_2O_3 inverse opals: synthesis and improved performance for acetone sensing toward diagnosis of diabetes, Nanoscale 7 (2015) 13051–13060.
[11] S.J. Choi, I. Lee, B.H. Jang, D.Y. Youn, W.-H. Ryu, C. Ook Park, I.D. Kim, Selective diagnosis of diabetes using Pt-functionalized WO_3 hemitube networks as a sensing layer of acetone in exhaled breath, Anal. Chem. 85 (2013) 1792–1796.
[12] N. Barsan, D. Koziej, U. Weimar, Metal oxide-based gas sensor research: How to?, Sens Actuators B: Chem 121 (2007) 18–35.
[13] L.A. Patil, D.R. Patil, Heterocontact type CuO-modified SnO_2 sensor for the detection of a ppm level H_2S gas at room temperature, Sens. Actuators B: Chem. 120 (2006) 316–323.
[14] I.C. Cosentino, E.N.S. Muccillo, R. Muccillo, The influence of Fe2O3 in the humidity sensor performance of ZrO_2: TiO_2-based porous ceramics, Mater. Chem. Phys. 103 (2007) 407–414.
[15] G.Y. Lu, J. Xu, J.B. Sun, Y.S. Yu, Y.Q. Zhang, F.M. Liu, UV-enhanced room temperature NO_2 sensor using ZnO nanorods modified with SnO_2 nanoparticles, Sens. Actuators B 162 (2012) 82–88.
[16] S.M. Wang, J. Cao, W. Cui, X.F. Li, D.J. Li, Facile synthesis and high acetone gas sensing performances of popcorn-like In_2O_3 hierarchical nanostructures, Mater. Lett. 186 (2017) 256–258.
[17] X.Q. Gao, X.T. Su, C. Yang, F. Xiao, J.D. Wang, X.D. Cao, S.J. Wang, L. Zhang, Hydrothermal synthesis of WO_3 nanoplates as highly sensitive cyclohexene sensor and high-efficiency MB photocatalyst, Sens. Actuators B 181 (2013) 537–543.
[18] J.B. Sun, P. Sun, D.L. Zhang, J. Xu, X.S. Liang, F.M. Liu, G.Y. Lu, Growth of SnO_2 nanowire arrays by ultrasonic spray pyrolysis and their gas sensing performance, RSC Adv. 4 (2014) 43429–43435.
[19] S. Norouz-Oliaee, A.A. Khodadadi, Y. Mortazavi, S. Alipour, Highly selective Pt/SnO_2 sensor to propane or methane in presence of CO and ethanol, using gold nanoparticles on Fe_2O_3 catalytic filter, Sens. Actuators B 147 (2010) 400–405.
[20] C.M. Aldao, F. Schipani, M.A. Ponce, E. Joanni, F.J. Williams, Conductivity in SnO_2 polycrystalline thick film gas sensors: tunneling electron transport and oxygen diffusion, Sens. Actuators B 193 (2014) 428–433.
[21] G. Cheng, K. Wu, P.T. Zhao, Y. Cheng, X.L. He, K.X. Huang, Controlled growth of oxygen-deficient tin oxide nanostructures via a solvothermal approach in mixed solvents and their optical properties, Nanotechnology 18 (2007) 355604.
[22] P. Sun, X.D. Mei, Y.X. Cai, J. Ma, Y.F. Sun, X.S. Liang, F.M. Liu, G.Y. Lu, Synthesis and gas sensing properties of hierarchical SnO_2 nanostructures, Sens. Actuators B 187 (2013) 301–307.
[23] W. Nakla, A. Wisitsora-at, A. Tuantranont, P. Singjai, S. Phanichphant, C. Liewhiran, H_2S sensor based on SnO_2 nanostructured film prepared by high current heating, Sens. Actuators B 203 (2014) 565–578.
[24] Y.C. Goswami, V. Kumar, P. Rajaram, V. Ganesan, M.A. Malik, P. O'Brien, Synthesis of SnO_2 nanostructures by ultrasonic-assisted sol-gel method, J. Sol-Gel Sci. Technol. 69 (2014) 617–624.
[25] J.R. Zhang, L. Gao, Synthesis and characterization of nanocrystalline tin oxide by sol-gel method, J. Solid State Chem. 177 (2004) 1425–1430.
[26] F. Song, H.L. Su, J. Han, D. Zhang, Z.X. Chen, Fabrication and good ethanol sensing of biomorphic SnO_2 with architecture hierarchy of butterfly wings, Nanotechnology 20 (2009) 495502.
[27] L. Cheng, S.Y. Ma, X.B. Li, J. Luo, W.Q. Li, F.M. Li, Y.Z. Mao, T.T. Wang, Y.F. Li, Highly sensitive acetone sensors based on Y-doped SnO_2 prismatic hollow nanofibers synthesized by electrospinning, Sens. Actuators B 200 (2014) 181–190.
[28] Y.G. Zheng, J. Wang, P.J. Yao, Formaldehyde sensing properties of electrospun NiO-doped SnO_2 nanofibers, Sens. Actuators B 156 (2011) 723–730.
[29] A.C. Bose, D. Kalpana, P. Thangadurai, S. Ramasamy, Synthesis and characterization of nanocrystalline SnO_2 and fabrication of lithium cell using nano-SnO_2, J. Power Sources 107 (2002) 138–141.
[30] Z.W. Jiang, Z. Guo, B. Sun, Y. Jia, M.Q. Li, J.H. Liu, Highly sensitive and selective butanone sensors based on cerium-doped SnO_2 thin films, Sens. Actuators B 145 (2010) 667–673.
[31] We.H. Tan, J.F. Tan, L.R. Fan, Z.T. Yu, J. Qian, X.T. Huang, Fe_2O_3-loaded NiO nanosheets fo fast response/recovery and high response gas sensor, Sens. Actuators B 256 (2018) 282–293.
[32] V.K. Tomer, K. Singh, H. Kaur, M. Shorie, P. Sabherwal, Rapid acetone detection using indium loaded WO_3/SnO_2 nanohybrid sensor, Sens. Actuators B 253 (2017) 703–713.
[33] X.Y. Kou, C. Wang, M.D. Ding, C.H. Feng, X. Li, J. Ma, H. Zhang, Y.F. Sun, G.Y. Lu, Synthesis of Co-doped SnO_2 nanofibers and their enhanced gas-sensing properties, Sens. Actuators B 236 (2016) 425–432.
[34] R. Deng, X.T. Zhang, E. Zhang, Y. Liang, Z. Liu, H. Xu, S.K. Hark, Planar defects in Sn-doped single-crystal ZnO nanobelts, J. Phys. Chem. C 111 (2007) 13013–13015.
[35] C. Peng, J.J. Guo, M.R. Liu, Y.X. Zheng, T.T. Huang, D.J. Wu, Enhanced ethanol sensing properties based on Sm_2O_3-doped ZnO nanocomposites, RSC Adv. 4 (2014) 64093–64098.
[36] J.F. Martel, S. Jandl, B. Viana, D. Vivien, Crystal-field study of Sm^{3+} ions in Sm_2O_3, Sm^{3+}:Gd_2O_3 and Sm^{3+}: Y_2O_3, J. Phys. Chem. Solids 61 (2000) 1455–1463.
[37] M.A. Abdullah, S. Mika, D. Joydeep, Gadolinium doped tin dioxide nanoparticles: an efficient visible light active photocatalyst, J. Rare Earths 33 (2015) 1275–1283.
[38] Q. Zhou, C. Tang, S.P. Zhu, W.G. Chen, J. Li, Synthesis, characterization and sensing properties of Sm_2O_3 doped SnO_2 nanorods to C_2H_2 gas extracted from power transformer oil, Mater. Tech.: Adv. Perform. Mater. 31 (2016) 364–370.
[39] F.M. Liu, Y.Q. Zhang, Y.H. Yu, J. Xu, J.B. Sun, G.Y. Lu, Enhanced sensing performance of catalytic combustion methane sensor by using Pd nanorod/γ-Al_2O_3, Sens. Actuators B 160 (2011) 1091–1097.
[40] D.D. Lian, B. Shi, R.R. Dai, X.H. Jia, X.Y. Wu, Synthesis and enhanced acetone gas-sensing performance of $ZnSnO_3/SnO_2$ hollow urchin nanostructures, J. Nanopart. Res. 19 (2017) 401.
[41] D.L. Chen, X.X. Hou, T. Li, L. Yin, B.B. Fan, H.L. Wang, X.J. Li, H.L. Xu, H.X. Lu, R. Zhang, J. Sun, Effects of morphologies on acetone-sensing properties of tungsten trioxide nanocrystals, Sens. Actuators B 153 (2011) 373–381.
[42] P. Gao, H.M. Ji, Y.G. Zhou, X.L. Li, Selective acetone gas sensors using porous WO_3-Cr_2O_3 thin films prepared by sol-gel method, Thin Solid Films 520 (2012) 3100–3106.
[43] Y. Zeng, T. Zhang, M.X. Yuan, M.H. Kang, G.Y. Lu, R. Wang, H.T. Fan, Y. He, H.B. Yang, Growth and selective acetone detection based on ZnO nanorod arrays, Sens. Actuators B 143 (2009) 93–98.

[44] J. Shin, S.J. Choi, D.Y. Youn, I.D. Kim, Exhaled VOCs sensing properties of WO_3 nanofibers functionalized by Pt and IrO_2 nanoparticles for diagnosis of diabetes and halitosis, J. Electroceram. 29 (2012) 106–116.
[45] Z.Q. Jiang, R. Zhao, B.L. Sun, G.D. Nie, H. Ji, J.Y. Lei, C. Wang, Highly sensitive acetone sensor based on Eu-doped SnO_2 electrospun nanofibers, Ceram. Int. 42 (2016) 15881–15888.
[46] J.H. Sun, J. Guo, J.Y. Ye, B.J. Song, K.W. Zhang, S.L. Bai, R.X. Luo, D.Q. Li, A.F. Chen, Synthesis of Sb doping hierarchical WO_3 microspheres and mechanism of enhancing sensing properties to NO_2, J. Alloy. Compd. 692 (2017) 876–884.
[47] M.R. Alenezi, A.S. Alshammari, K.D.G.I. Jayawardena, M.J. Beliatis, S.J. Henley, S. R.P. Silva, Role of the exposed polar facets in the performance of thermally and UV activated ZnO nanostructured gas sensors, J. Phys. Chem. C 117 (2013) 17850–17858.

Yiqun Zhang received the BE degree in Department of Electronic Sciences and Technology in 2009. She is currently studying for her Dr Sci degree in College of Electronic Science and Engineering, Jilin University, China.

Linsheng Zhou received the BS degree in Department of Electronic Science and Technology in 2017. He is currently studying for his M.E Sci degree in College of Electronic Science and Engineering, Jilin University, China.

Yueying Liu received the BS degree in Department of Micro-Electronics in 2017. She is currently studying for her M.E Sci degree in College of Electronic Science and Engineering, Jilin University, China.

Deye Liu received the BS degree in Department of Micro-Electronics in 2011. He is currently studying for his M.E Sci degree in College of Electronic Science and Engineering, Jilin University, China.

Fengmin Liu received the BE degree in Department of Electronic Science and Technology in 2000. She received her Doctor's degree in College of Electronic Science and Engineering at Jilin University in 2005. Now she is an professor in Jilin University, China. Her current research is preparation and application of semiconductor oxide, especial in gas sensor and solar cell.

Fangmeng Liu received his PhD degree in 2017 from College of Electronic Science and Engineering, Jilin University, China. Now he is a lecturer of Jilin University, China. His current research interests include the application of functional materials and development of solid state electrolyte gas sensor and flexible device.

Xu Yan received his M.S degree in 2013 from Nanjing Agricultural University. He joined the group of Prof. Xingguang Su at Jilin University and received his Ph.D. degree in June 2017. Since then, he did postdoctoral work with Prof. Geyu Lu and Prof. Junqiu Liu. Currently, his research interests mainly focus on the development of the functional nanomaterials for chem/bio sensors.

Xishuang Liang received the BE degree in Department of Electronic Science and Technology in 2004. He received his Doctor's degree in College of Electronic Science and Engineering at Jilin University in 2009. Now he is an associate professor of Jilin University, China. His current research is solid electrolyte gas sensor.

Yuan Gao received her PhD degree from Department of Analytical Chemistry at Jilin University in 2012. Now she is an associate professor in Jilin University, China. Her current research is focus on the preparation and application of graphene and semiconductor oxide, especial in gas sensor and biosensor.

Geyu Lu received the B.Sci. degree in Electronic Sciences in 1985 and the M.Sci. degree in 1988 from Jilin University in China and the Dr.Eng. degree in 1998 from Kyushu University in Japan. Now he is a professor of Jilin University, China. His current research interests include the development of chemical sensors and the application of the function materials.